Journal of Visualization, Vol. 7, No. 2 (2004) 119-126

Effect of Elasticity of a Polymer Solution on the Hele-Shaw Flow

Win Shwe Maw *, Shingo Fujiwara * , Tsutomu Takahashi * and Masataka Shirakashi *

* Department of Mechanical Engineering
Nagaoka University of Technology, Kamitomiokamachi 1603-1, Nagaoka, Japan.
Phone: +81-258-47-9730, Fax: +81-258-47-9770
E-mail: kashi@mech.nagaokaut.ac.jp

Received 13 May 2003
Revised 6 August 2003

Abstract : In this study, the Hele-Shaw cell is used to examine the effect of fluid elasticity on the flow patterns of two-dimensional potential flow. Flows around a circular cylinder, a square cylinder and flows through abruptly converging-diverging channels (slits) with different throat lengths are tested for water and 0.2 wt % polyacrylamide aqueous solution (PAA-solution). The viscosity of the latter is well modeled by the power law, and the first normal stress difference in the steady shear flow is around ten times higher than the shear stress. Although the PAA-solution is highly shear-thinning, the flows of PAA-solution well reproduce the two-dimensional potential flow patterns that correspond to the respective flow configurations when the flow rate is very low. The potential flow patterns of PAA solution are disturbed in the opposite way of inertia effect observed for water. The streamlines near the upstream stagnation point of cylinders are shifted upstream separating from the cylinder surface when the flow rate is higher, while streamlines in the wake approach closer to the downstream stagnation point. Streamlines of flow through the slit at flow rates higher than the potential flow region show that a pair of vortices is formed upstream the slit entrance, while the streamlines remain attached to the downstream wall after passing the slit.

Keywords : Hele-Shaw flow, Viscoelastic fluid, Flow around a cylinder, Converging-diverging channel, Weissenberg number

1. Introduction

It is of practical importance in polymer processing and engineering to predict flow behaviors of viscoelastic fluids. The effect of elasticity of fluids are the most prominent in extensional flows of polymeric materials such as flows in spinning, injection and coating (Boger, 1987, 1993), (Larson, 1992). All of rheology models proposed so far are constituted to take both viscosity and elasticity into account since they always come together for any polymeric material or polymer solution. However, Hasegawa (1997) suggested that mechanisms of some peculiar phenomena in polymer solution flows could be explained by applying the Bernoulli's theorem extended to include elastic stresses. This suggestion leads to a new concept of "inviscid elastic fluid model", meaning that effect of viscosity of a polymer solution can be neglected in flows where elasticity is dominant.

The Hele-Shaw cell is a channel between two transparent parallel plates with a small separation (Itaya, 1966). When a plate of an arbitrary configuration is inserted between the two plates so that it completely fills the gap, the resulting pattern of streamlines is identical with that in

the two-dimensional potential flow with the same boundary geometry, provided that the fluid is Newtonian and the inertia force is negligible (Schlichting, 1979), (Van Dyke, 1982). Since the two-dimensional potential flow pattern is obtained theoretically for incompressible inviscid fluid, it would be effective to investigate the influence of fluid elasticity on the Hele-Shaw flow in order to understand the behavior of "inviscid elastic fluid". However, there are only a few reports on the Hele-Shaw flow of non-Newtonian fluid (e.g., Yamamoto, 2001). In this study, the Hele-Shaw cell is used to examine the effect of elasticity on the flow patterns of two-dimensional potential flows with several boundary geometries.

2. Experimental Apparatus and Test Fluids

2.1 Hele-Shaw Cell and Configurations of Cylinders and Converging-Diverging Channels

The dimensions of the Hele-Shaw cell channel are 140 mm width, 200 mm length and the gap between two plates $2h$ is 1 mm (Fig. 1). Test fluid added with small amount of dye is introduced from an array of thin capillaries to form parallel streak lines in the Hele-Shaw cell when the flow is not disturbed. In this study, black Japanese calligraphic ink (so called commercial Bokujuu) is added to each sample liquid with 0.3 wt % concentration. A circular plate with a diameter d = 25 mm and a square plate of a side length d = 25 mm are used as the test cylinders. Two abruptly converging-diverging channels with an equal opening d = 10 mm and different lengths L = 10 mm and 2 mm as shown in Fig. 2 are used to observe flows passing through a slit.

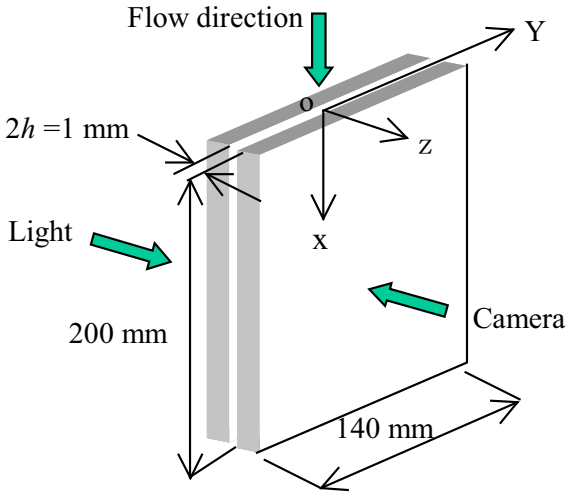

Fig. 1. Hele-Shaw Cell Apparatus and the Coordinate System.

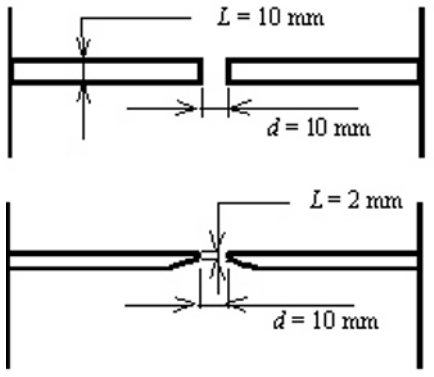

Fig. 2. Converging-Diverging Channels.

2.2 Fluids and Parameters

Water is used as a Newtonian fluid and a 0.2 wt % polyacrylamide aqueous solution (PAA-solution) as a viscoelastic fluid. The shear viscosity η , the shear stress σ and the first normal stress difference N_1 of the PAA -solution in the steady shear flow are shown in Fig. 3 plotted against the shear rate $\dot{\gamma}$. The PAA-solution has a shear thinning viscosity that is well modeled by the power-law fluid over a shear rate range from 10^{-1} to 10^{2} 1/s, and no degradation was found in the shear stress and the first normal stress difference data after an experimental run.

When the power law model

$$\sigma = K\dot{\gamma}^n \tag{1}$$

is applied to the shear stress of PAA-solution, the shear rate on the wall in the free flow of the Hele-Shaw cell is given by

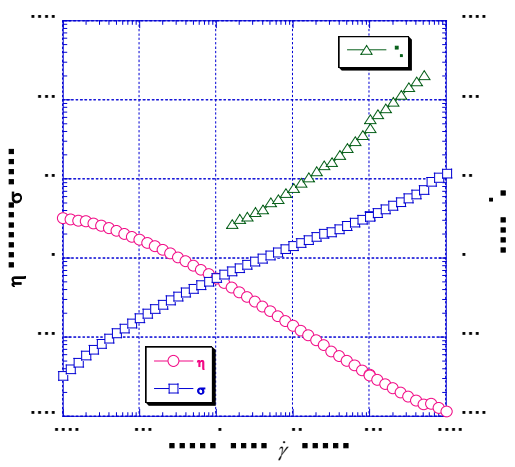

Fig. 3. Rheological Properties of PAA-Solution in Steady Shear Flow (Viscosity η, the First Normal Stress Difference N_1, Shear Stress σ vs. Shear Rate $\dot{\gamma}$).

$$\dot{\gamma}_w = \frac{n+1}{n}.\frac{V_{\max}}{h}, \tag{2}$$

where $V_{\max}$ is the maximum velocity, i.e. the center line velocity of the Hele-Shaw cell. Hence, the Reynolds number Re defined as the ratio of the inertia force to the shear stress on the wall is,

$$Re = \frac{\rho V d}{[\eta]_w}\left(\frac{h}{d}\right)^2, \tag{3}$$

where $[\eta]_w$ is the viscosity at $\dot{\gamma} = \dot{\gamma}_w$, V is the mean velocity and h is the half of the gap.

3. Observations of Flow Patterns

3.1 Flow around Circular Cylinder

Figure 4 shows photographs of water flows around the circular cylinder at a very low Reynolds number and a higher value of Re. The direction of flow is downward in all the photographs in this paper. Fig. 4(a) shows that the Hele-Shaw flow of a Newtonian fluid reproduces the two-dimensional potential flow pattern when Re<0.16 When the flow rate is increased and Re becomes close to the order of unity, the flow separates near the maximum width position of the cylinder and wake is formed behind it as shown in Fig. 4(b).

The behavior of PAA- solution flow with increasing flow rate is quite opposite of water, as seen in Fig. 5. The flow pattern at a very low flow rate as in Fig. 5(a) is identical with the potential pattern as in the case of water at low Re. When the flow rate is increased, the streamlines are shifted further from the upstream stagnation point and they approach closer to the downstream stagnation point, as seen in Fig. 5(b). Similar phenomenon is reported in a two-dimensional flow, i.e. flow of a polymer solution around a circular cylinder with fairly large span-wise length (Menaro and Mena, 1981).

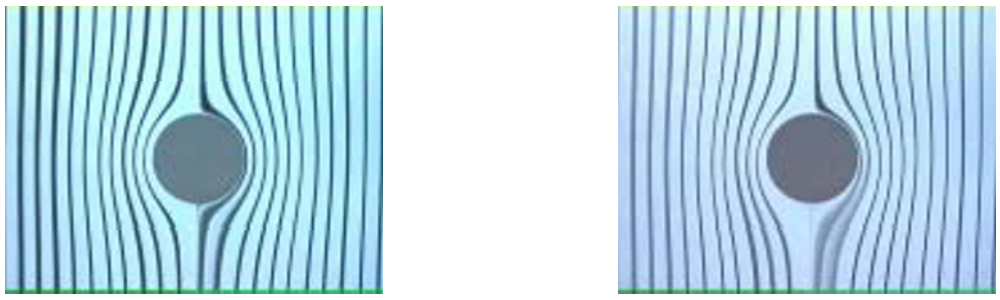

(a) $Re = 1.63\text{x}10^{-1}$, $\dot{\gamma}_w = 9.80\text{x}10^{1}(1/s)$ (b) $Re=5.32\text{x}10^{-1}$, $\dot{\gamma}_w=3.20\text{x}10^{2}(1/s)$

Fig. 4. Flow of Water around Circular Cylinder.

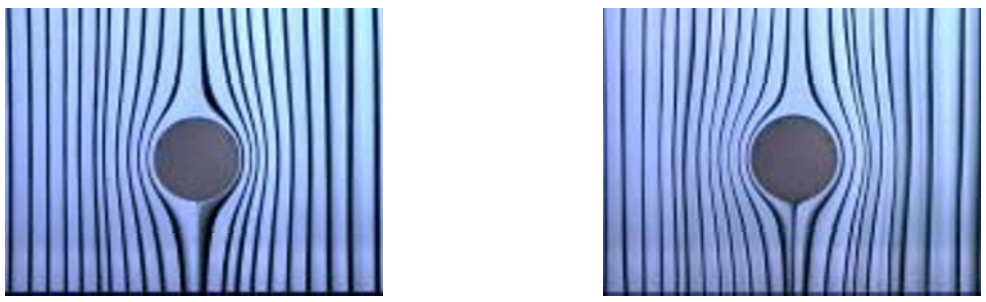

(a) $Re=2.54\ \text{x}10^{-4}$, $\dot{\gamma}_w= 1.92\text{x}10^{1}(1/s)$ (b) $Re=6.94\text{x}10^{-3}$, $\dot{\gamma}_w=1.65\text{x}10^{2}(1/s)$

Fig. 5. Flow of PAA-Solution around Circular Cylinder.

3.2 Flow around Square Cylinder

Figure 6 shows flow patterns of water around the square cylinder. When *Re* is very low, the potential flow pattern is reproduced as in Fig. 6(a). When *Re* is higher, such as $Re \approx 1$, the water flow around the square cylinder separates at the edges and forms a pair of vortices in the wake due to inertia effect, while the streamlines remain attached on the front surface.

In flows of PAA-solution, effect of elasticity similar to that observed for the circular cylinder is more clearly seen for the flows around the square as shown in Fig. 7. The symmetric potential flow pattern is reproduced at the lowest flow rate as in Fig. 7(a). It is disturbed into asymmetric between upstream and downstream in a similar way as in the case of the circular cylinder when the flow rate is increased (Fig. 7(b)). When the flow rate is still increased, a vortex similar to the lip vortex observed in the slit entry flow (Boger, 1993) forms at each front edge of the square as seen in Fig. 7(c).

(a) $Re=1.04\ \text{x}\ 10^{-1}$, $\dot{\gamma}_w=6.23\ \text{x}\ 10^{1}$ (1/s) (b) $Re=9.39\ \text{x}\ 10^{-1}$, $\dot{\gamma}_w=5.66\ \text{x}\ 10^{2}(1/s)$

Fig. 6. Flow of Water around Square Cylinder.

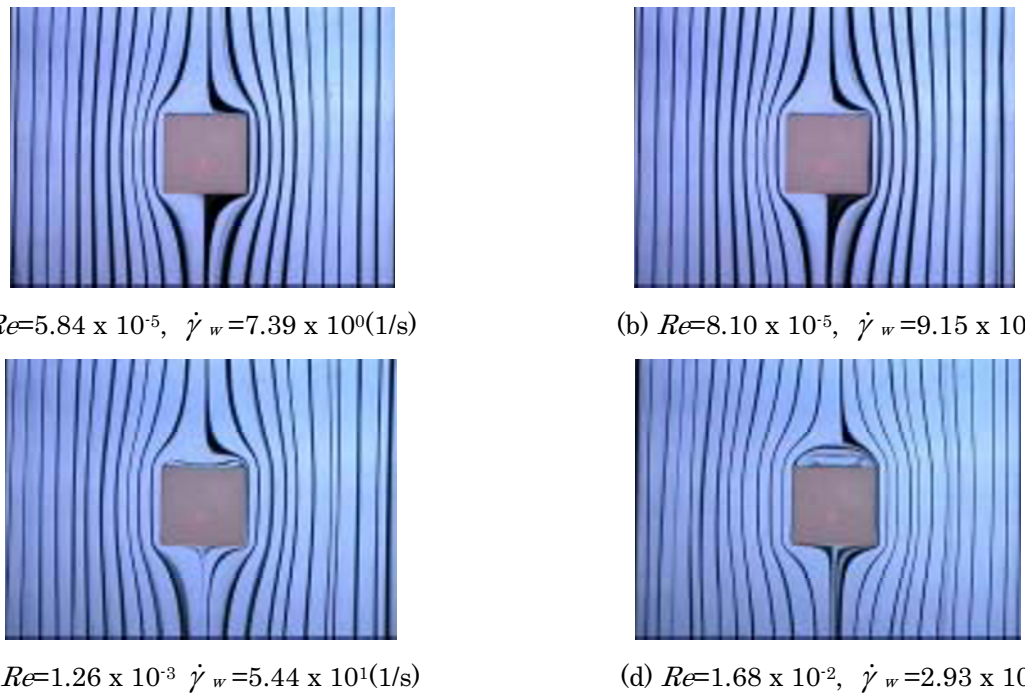

(a) Re=5.84 x 10^{-5}, $\dot{\gamma}_w$=7.39 x 10^{0}(1/s) (b) Re=8.10 x 10^{-5}, $\dot{\gamma}_w$=9.15 x 10^{0}(1/s)

(c) Re=1.26 x 10^{-3} $\dot{\gamma}_w$=5.44 x 10^{1}(1/s) (d) Re=1.68 x 10^{-2}, $\dot{\gamma}_w$=2.93 x 10^{2}(1/s)

Fig. 7. Flow of PAA-Solution around Square Sylinder.

These vortices grow with increasing flow rate and coalesce to form a considerably large convex bubble on the front surface as shown in Fig. 7(d). It should be noted that the Reynolds number in Fig. 7(d) is low enough to take the inertia effect negligible and that the streamlines attach to the rear surface approaching to the stagnation point closer than those in Fig. 7(a).

3.3 Flow Passing through Slit

Fig. 8 shows flow patterns of water passing through the slit with L/d=1. When Re is low as in Fig. 8 (a), the flow pattern is symmetrical between upstream and downstream, with no separation over the whole flow field, resulting in the potential flow pattern. When the Re is higher, the flow passing the slit forms a jet-like pattern as seen in Fig. 8(c) due to inertia effect.

The effect of fluid elasticity in the slit flow is quite opposite to the inertia effect. When the flow rate is low, the flow pattern of PAA-solution is very similar to the potential flow (Figs. 9(a) and 10 (a)). When the flow rate is increased, a pair of lip vortices is formed at both sides of the slit entrance, while the streamlines remain attached to the wall at the downstream section as seen in Figs. 9(b) and 10(b). The size of lip vortex at the slit entrance increases with flow rate. The height and width of vortex are measured from many photos and plotted against $\dot{\gamma}_w$, the wall shear rate, for the two slit flows. In spite that the vortex size scatters due to the arbitrary nature of measurement, no significant difference was observed between the average vortex sizes for the two slits.

(a) Re=6.98 x 10^{-2}, $\dot{\gamma}_w$=1.68 x 10^{1}(1/s) (b) Re=2.58 x 10^{-1}, $\dot{\gamma}_w$=6.22 x 10^{1}(1/s) (c) Re=1.12 x 10^{0}, $\dot{\gamma}_w$=2.71 x 10^{2}(1/s)

Fig. 8. Flow of Water Passing through the Abruptly Converging-Diverging Channel (L/d=1).

(a)Re=1.63 x 10^{-5}, $\dot{\gamma}_w$=1.78 x 10^0 (1/s) (b)Re=1.37 x 10^{-4}, $\dot{\gamma}_w$=7.10 x 10^0 (1/s) (c)Re=1.39 x 10^{-2}, $\dot{\gamma}_w$=1.43 x 10^2 (1/s)

Fig. 9. Flow of PAA-Solution Passing through the Abruptly Converging-Diverging Channel (L/d=1).

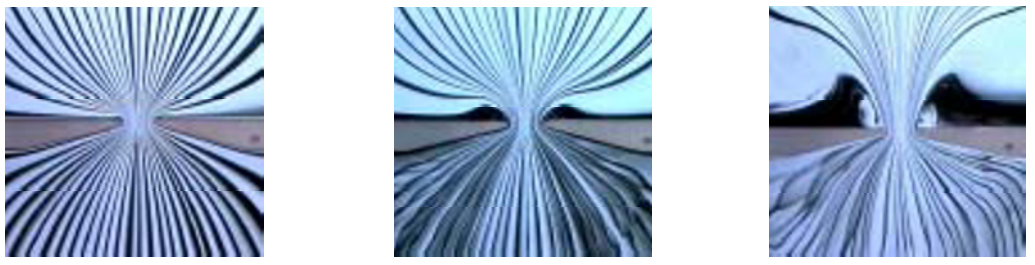

(a) Re=1.00 x 10^{-5}, $\dot{\gamma}_w$=1.30 x 10^0 (1/s) (b) Re=1.88 x 10^{-4}, $\dot{\gamma}_w$=8.72 x 10^0 (1/s) (c) Re=1.19 x 10^{-2}, $\dot{\gamma}_w$=1.29 x 10^2 (1/s)

Fig. 10. Flow of PAA-Solution Passing through the Abruptly Converging-Diverging Channel (L/d=0.2).

4. Discussions on the Flow Pattern

In the case of water, streaks are blurred and diffused where the inertia effect is dominant, such as in Figs. 4(b), 6(b) and 8(b) (c), showing that the streamlines on planes with different z-coordinate do not coincide each other. Whereas, the streaks of the PAA-solution at high flow rates keep definite contour even when the flow pattern is disturbed due to elastic effect as seen in Figs. 7(d), 9(c) and 10 (c).

Since the deviation of streak patterns from the potential streamlines is most clearly seen in their asymmetry between the upstream and the downstream, the onset of disturbance on symmetry was examined to find the critical flow rate for the potential flow analogy. The maximum flow rate for the potential flow pattern and the minimum flow rate for disturbed flows are determined from numerous photographs obtained for various flow rates.

The results of water are given in Table 1, where the characteristic velocity, Reynolds number and the wall shear rate corresponding to the critical flow rates are presented. The real critical values should be somewhere between the maximum potential flow and the minimum disturbed flow values. From Table 1, the critical Reynolds number $[Re]_c$ for water is known to be considerably lower than unity, say around 0.2, for the circular and the square cylinder, and around 0.1 for the slit flow maybe due to the higher velocity through the slit.

The results of the PAA-solution are presented in Table 2, where the relaxation time λ and the Weissenberg number We determined from the data of steady shear flow in Fig. 3 by the following equations are also added. The value of $[Re]_c$ for the PAA-solution estimated from the data in Table 2 is more than two decades lower than that of water for all the geometries, which indicates that the onset of deviation from potential pattern occurs well in creeping flow region.

$$\lambda = \frac{N_1}{2\sigma\dot{\gamma}} \tag{4}$$

$$We = \frac{\lambda V}{d} \tag{5}$$

For the Hele-Shaw flow, it seems plausible to assume that the z-component of velocity is negligible. If we assume, furthermore, that the profiles of both x- and y-velocity components in the z-direction are similar to inelastic non-Newtonian viscosity fluids, like the case for Newtonian fluids, it is proved that the flow pattern reproduces the potential flow. Since the critical shear rates of the PAA-solution indicated from data in Table 2 are well in the shear-thinning range, it is concluded that the above assumptions are acceptable when the elastic effect is negligible.

The common feature of elastic effect is that the streak lines are likely to be detached from the body wall in the region of converging stream lines, and they are likely to be attached to the wall in the region of diverging streamlines such as in the wake of cylinder or exit of the slit. This effect is opposite to the inertia so that one might take the flow direction upward in Figs. 9(c) and 10 (c).

For the PAA-solution, the potential flow pattern is obtained over a range of wall shear rate $\dot{\gamma}_w$ where the N_1 is quite large, e.g. in the case of the circular cylinder the potential flow analogy holds up to $\dot{\gamma}_w = 2.88\times10^1$ 1/s from Table 2 and the ratio $N_1/\sigma \approx 10$ at this value of $\dot{\gamma}_w$ as seen in Fig. 3. Although the first normal stress difference N_1 gives a measure of elasticity, this fact shows that its effect on the potential flow pattern can be taken to be insignificant.

Therefore, it is inferred that the deviation from the potential pattern of the PAA-solution flow is attributed to the elongational stress generated in the flow where the streamlines are converging. The Weissenberg number *We* can be a measure to know the condition for potential flow analogy. However, *We* in Table 2 cannot be a reasonable criterion since it is based on the steady shear flow measurement. Measurements on relaxation time in elongational flow and experiments on fluids with different relaxation time are needed to assure if it can give the criterion for the potential flow analogy.

Table 1. Critical Velocity, Shear Rate and Reynolds Number of Water Flow.

	Circular Cylinder		Square Cylinder		Slit (L/d=1)	
	max. potential	min. disturbance	max. potential	min. disturbance	max. potential	min. disturbance
V (m/s)	2.20×10^{-2}	2.26×10^{-2}	1.55×10^{-2}	2.48×10^{-2}	2.80×10^{-3}	4.09×10^{-3}
$\dot{\gamma}_w$ (1/s)	1.32×10^{2}	1.36×10^{2}	9.30×10^{1}	1.49×10^{2}	1.68×10^{1}	2.45×10^{1}
Re (-)	2.19×10^{-1}	2.25×10^{-1}	1.54×10^{-1}	2.47×10^{-1}	6.98×10^{-2}	1.02×10^{-1}

Table 2. Critical Velocity, Shear Rate, Reynolds Number, Relaxation Time and Weissenberg Number of 0.2 wt% PAA-Solution.

	Circular Cylinder		Square Cylinder		Slit (L/d=1)		Slit (L/d=0.2)	
	max. potential	min. disturbance	max. potential	min. disturbance	max. potential	min. disturbance	max. potential	min. disturbance
V (m/s)	3.45×10^{-3}	4.67×10^{-3}	1.53×10^{-3}	2.19×10^{-3}	2.14×10^{-4}	3.25×10^{-4}	1.76×10^{-4}	4.20×10^{-4}
$\dot{\gamma}_w$ (1/s)	2.88×10^{1}	3.89×10^{1}	1.27×10^{1}	1.83×10^{1}	1.78×10^{0}	2.71×10^{0}	1.47×10^{0}	3.51×10^{0}
Re (-)	4.73×10^{-4}	7.52×10^{-4}	1.35×10^{-4}	2.36×10^{-4}	1.63×10^{-5}	3.11×10^{-5}	1.22×10^{-5}	4.62×10^{-5}
λ (s)	0.15	0.12	0.27	0.21	1.03	0.77	1.17	0.65
We (-)	2.09×10^{-2}	2.29×10^{-2}	1.62×10^{-2}	1.82×10^{-2}	2.20×10^{-2}	2.51×10^{-2}	2.07×10^{-2}	2.72×10^{-2}

5. Conclusion

The potential flow pattern analogy by the Hele-Shaw cell is shown to hold for the PAA-solution when the flow rate is low in spite of its highly shear-thinning viscosity and the considerably large value of

the first normal stress difference in shear flow. When the flow rate is higher than this potential pattern region, elasticity of the PAA-solution changes the flow pattern in a way opposite to the inertia force effect.

The streamlines of the PAA-solution approach closer to the stagnation point behind the cylinder, where the inertia causes the flow separation when the fluid is inelastic. Streamlines through a slit at flow rates higher than the potential flow region show that a pair of vortices is formed on both sides of the slit entrance, while the flow expands over the whole channel width after passing the slit. This effect of elasticity is considered to be caused by elongational stress of the PAA-solution since it is most clearly observed in flows where streamlines are converging or diverging.

References

Boger, D. V., Viscoelastic Flow through Contraction, Annual Review of Fluid mechanics, 19 (1987), 157-182.
Boger, D. V. and Walters, K., Rheological Phenomena in Focus, Elsevier, Amsterdam, The Netherlands. (1993)
Hasegawa, T., Generalization of Bernoulli's Theorem for an Elastic Fluid and its Application to Some Flow Problems, Nihon Reoroji Gakkaishi, 25-4 (1997), 211-214. (in Japanese)
Itaya, M., Chapter 4. Principles on Motions of Water, Suirikigaku, Asakura, 66 (1966). (in Japanese)
James, D. F. and Walters, K., Critical Appraisal of Available Methods for the Measurement of Extensional Properties of Mobile System, Techniques in Rheological Measurement, Ed. By Collyer, A. A., Chapman & Hall, London. (1993) 33-53.
Larson, R. G., Instabilities in Viscoelastic Flow, Rheologica Acta, 31 (1992), 213-263.
McGlashan, S. A. and McKay, M. E., Comparison of Entry Flow Techniques for Measuring Elongation Flow Properties, J. Non-Newtonian Fluid Mech., 85 (1999), 213-227.
Menaro, O. and Mena, B., On the Slow Flow of Viscoelastic Liquids past a Circular Cylinder, J. Non-Newtonian Fluid Mech., 9 (1981), 379-387.
Schlichting, H., Boundary Layer Theory, 7th ed., McGraw-Hill, New York. (1979), 123-125.
Van Dyke, M., An Album of Fluid Motion, The Parabolic Press, Stanford, California. (1982) 8.
Yamamoto, T., Kamikawa, H., Tanaka, H., Nakamura, K. and Mori, N., Viscous Fingering of Non-Newtonian Fluids in a Rectangular Hele-Shaw Cell, Nihon Reoroji Gakkaishi, 29-2 (2001), 81-87.

Author Profile

Masataka Shirakashi: He received his M. Eng. and Dr. Eng. from Tokyo Institute of Technology in the year of 1969 and 1978, respectively. He has been working for Nagaoka University of Technology since 1978 in the Department of Mechanical Engineering, as an associate professor from 1978 to 1990 and as a professor since 1990. His research interests are Flow Induced Vibration, Viscoelastic Fluid Flow and Utilization of Ice or Snow/ Water Slurry for Cooling Energy Transportation.

Tsutomu Takahashi: He received his M. Eng. and Dr. Eng. from Science University of Tokyo in the year of 1986 and 1989, respectively. He has been working for Nagaoka University of Technology since 1990 in the Department of Mechanical Engineering, as a research associate from 1990 to 1995 and an associate professor since 1996. His research interests are Viscoelastic Fluid Flow, Optical Rheometry and Flow Induced Vibration.

Win Shwe Maw: She received her M.E. (Mech.) degree in Mechanical Engineering in 1999 from Yangon Technological University, Myanmar. Now she is studying Rheology in Mechanical Engineering Department, Nagaoka University of Technology, Japan for her doctorate course. Her current research works are concerning with Hele-Shaw Flow, Abruptly Contracting Channel Flows Using Flow Visualization Methods and Laser Doppler Velocimetry.

Shingo Fujiwara: He received his B.E. (Mech.) degree in Mechanical Engineering in 2002 from Nagaoka University of Technology, Japan. Now he is studying Rheology in the same university for his master degree. His current research works are concerning with Hele-Shaw Flow and Photochromic Visualization Method.